ACS NANO
Cite This: ACS Nano 2018, 12, 5699–5708
www.acsnano.org

ARTICLE

Multifluorophore DNA Origami Beacon as a Biosensing Platform

Denis Selnihhin,[†,‡] Steffen Møller Sparvath,[†,‡] Søren Preus,[†,§] Victoria Birkedal,[†,§] and Ebbe Sloth Andersen*[,†,‡]

[†]Center for DNA Nanotechnology, Interdisciplinary Nanoscience Center, [‡]Department of Molecular Biology and Genetics, and [§]Department of Chemistry, Aarhus University, 8000 Aarhus, Denmark

Supporting Information

ABSTRACT: Biosensors play increasingly important roles in many fields, from clinical diagnosis to environmental monitoring, and there is a growing need for cheap and simple analytical devices. DNA nanotechnology provides methods for the creation of sophisticated biosensors, however many of the developed DNA-based sensors are limited by cumbersome and time-consuming readouts involving advanced experimental techniques. Here we describe design, construction, and characterization of an optical DNA origami nanobiosensor device exploiting arrays of precisely positioned organic fluorophores. Two arrays of donor and acceptor fluorophores make up a multifluorophore Förster resonance energy-transfer pair that results in a high-output signal for microscopic detection of single devices. Arrangement of fluorophores into arrays increases the signal-to-noise ratio, allowing detection of signal output from singular biosensors using a conventional fluorescence microscopy setup. Single device analysis enables detection of target DNA sequences in concentrations down to 100 pM in <45 min. We expect that the presented nanobiosensor can function as a general platform for incorporating sensor modules for a variety of targets and that the strong signal amplification properties may allow detection in portable microscope systems to be used for biosensor applications in the field.

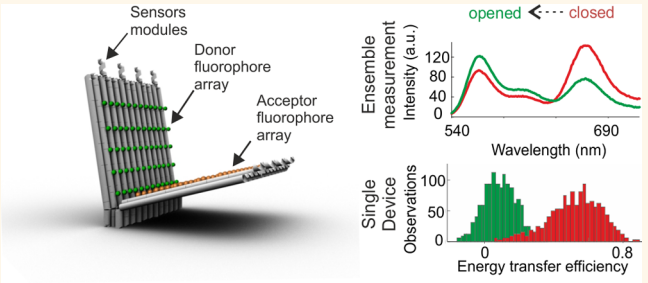

KEYWORDS: *DNA origami, DNA nanotechnology, biosensors, multifluorophore networks, energy transfer*

Biosensors are analytical tools that convert a biochemical reaction or process into a more easily readable output signal. It consists of two components: a biorecognition element that is responsible for detection of the biochemical reaction upon recognition of an analyte of interest and a transducer that converts the biorecognition event into a readily detectable signal: optical, electrical, calorimetric, *etc*. Biosensors have been developed for detection of many different molecules and reactions, for example, small molecules,[1−3] enzymes and enzymatic activity,[4,5] proteins,[6,7] and protein conformational change.[8] Many biosensor transducers are based on spectroscopic techniques, but due to a low signal-to-noise ratio of individual biosensors, the output signal is generated as an ensemble measurement, which represents an average state of all biosensor devices in the sample. Increasing the intensity of the spectroscopic output signal of the individual biosensors will allow the detection of these on a single device level and possibly be used with cheap and portable bright-field and fluorescence microscopes that have been developed to assist on-site analysis.[9,10] The recent point-of-care devices take advantage of mobile phone processors and optics as read out platforms and can thus provide a cost-effective alternative to expensive diagnostic technology.[11−13] However, the lack of sensitivity compared to dedicated stand-alone microscopes can limit the use of these systems. One of the solutions has been to use high-intensity fluorescence emitters such as quantum dots to develop single molecule biosensors.[14,15] Alternatively, gold and silver nanoparticles can be used to create a plasmonic hotspot for fluorescence enhancement,[16] which has been used to create a single-molecule biosensor allowing for label-free detection of Zika virus nucleic acids by single-molecule custom-built confocal microscope.[17] Another approach to increase the fluorescence intensity of a single biosensor device is to organize fluorophores into precisely positioned fluorophore networks and implement such networks into a transducer element of a biosensor device. Such precise organization of fluorophores and other small molecules is possible using DNA nanotechnology.[18]

DNA nanotechnology and especially the DNA origami method allow construction of nanoscale structures of almost arbitrary shapes in 2D[18,19] and 3D[20,21] that can be further developed into dynamic nanodevices.[22−26] The ability of DNA

Received: February 26, 2018
Accepted: May 15, 2018
Published: May 15, 2018

DOI: 10.1021/acsnano.8b01510
ACS Nano 2018, 12, 5699–5708

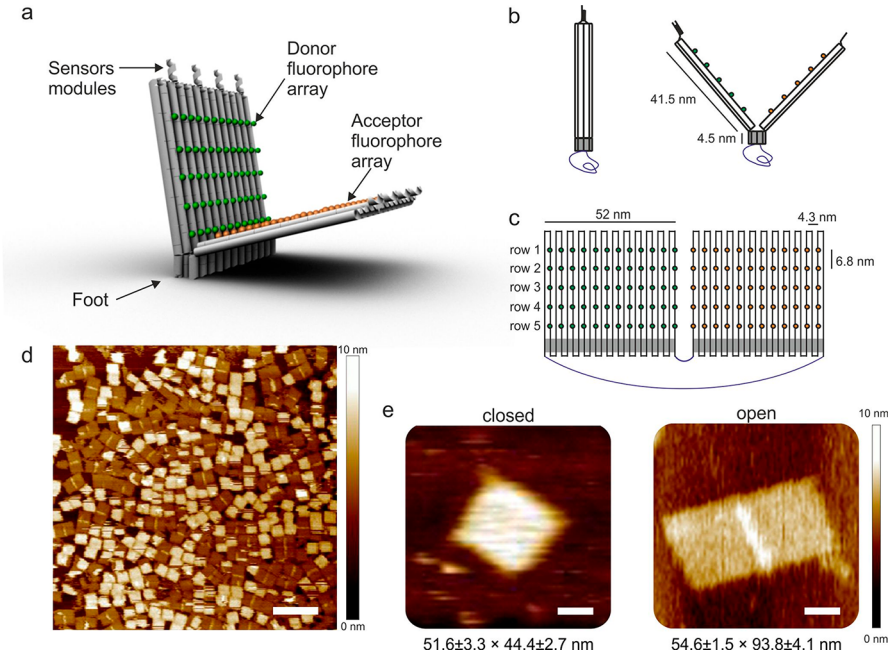

Figure 1. Design of the DNA origami multifluorophore beacon. (a) 3D model of the beacon with a multifluorophore FRET pair consisting of 60 donors (green spheres) and 60 acceptors (orange spheres). (b) Side-view of the beacon in the closed and open state. Dimensions of the foot and panels are shown. (c) Scaffold strand path. The foot is colored gray, and the blue line indicates the long single-stranded loop. Green and orange circles represent the arrangement of fluorophores in the donor and acceptor arrays, respectively. Distances between fluorophores in the row and between the rows are indicated. (d) AFM image of the self-assembled beacon at 12 mM Mg^{2+}, scale bar 200 nm. (e) AFM images of individual beacons in the closed and open states with their average size (n = 20), scale bars 20 nm.

nanotechnology to create nanostructures that can arrange fluorophores with high spatial accuracy was used to create simple fluorophore networks[27] and mimic biological light-harvesting complexes[28,29] to study dipolar interactions between multiple fluorophores. Precise positioning of multiple fluorophores has been used to create Förster resonance energy-transfer (FRET)-based photonic networks and wires to study multidye FRET cascades and homoFRET.[29,30] Linear FRET arrays have been used to create a multitarget detection system with an ensemble FRET readout.[31] One of the earliest examples of using DNA to build a biosensor is the molecular beacon from Tyagi and Kramer.[32] With the advancement of DNA nanotechnology, more complex DNA structures have been fabricated for biosensing purposes. One of the first was a microRNA (miRNA) sensing platform consisting of a flat DNA origami where miRNAs hybridized and could be imaged by atomic force microscopy (AFM).[33] A flat DNA origami was also used to detect the enzymatic activity of human O^6-alkylguanine-DNA alkyltransferase (hAGT), where the result of the enzymatic activity was imaged by AFM.[34] Kuzuya and colleagues presented another example of a single-molecule detection platform with a DNA origami forceps structure that changed its conformation upon binding of different analytes, where the conformational change could be visualized by AFM.[35] A seesaw-like DNA origami nanostructure was used to analyze hybridization of oligonucleotides by imaging the conformation of the structure by TEM.[36] A DNA walker assay was shown to act as a linear fluorescence amplifier for the detection of a specific oligonucleotide, where the walker path could be sandwiched in a hotspot of two gold nanoparticles allowing further fluorescent enhancement.[37] A DNA origami force clamp was used to study the holiday junction conformational transition and bending of a DNA helix by a TATA-box binding that was followed by an output signal of a single FRET pair.[38] All the devices demonstrated detection at the single-device level by means of AFM, TEM, or single-molecule microscopy techniques. Although these are powerful tools for direct visualization of nanodevices, the data acquisition process is cumbersome and slow. Furthermore, the detection systems are bulky, and it is currently not possible to turn them into point-of-care devices.

Here, we present a dynamical DNA origami device, consisting of two multifluorophore donor and acceptor arrays each consisting of up to 60 fluorophores. We use DNA origami to self-organize organic fluorophores into ordered multifluorophore arrays and use these arrays as a multifluorophore FRET pair. The multifluorophore FRET beacon resembles an enhanced molecular beacon with a high intensity output signal, which allows single-device analysis using a mainstream fluorescence microscope. We demonstrate the ability of the device to detect small oligonucleotides in concentrations down to 100 pM with a detection time of 2 min. The benefit of the developed DNA origami beacon is that the sensor modules can be easily exchanged for detection of different nucleotide sequences or by aptamer-based sensor modules, allowing detection of small molecules and proteins.

RESULTS AND DISCUSSION

Design of DNA Origami Beacon Devices. Inspired by the original molecular beacon,[32] we wanted to use the DNA origami method to construct a beacon that would provide a high-intensity output signal enabling detection of single devices in a simple fluorescence microscopy setup. The main idea was to employ arrays of donor and acceptor fluorophores in a DNA origami device to create a multifluorophore FRET pair that will result in a multiplied fluorescence output. The DNA origami

DOI: 10.1021/acsnano.8b01510
ACS Nano 2018, 12, 5699−5708

beacon was designed using caDNAno[39] and consists of two rectangular panels connected at the bottom by a foot and by a set of sensor modules at the top (Figure 1a). Each panel has an array of precisely positioned fluorophores: one array with donor fluorophores and the other array with corresponding acceptor fluorophores creating a multifluorophore FRET pair. Each fluorophore array consists of 5 rows with 12 fluorophores per row, resulting in up to 60 FRET pairs per device. The distance between two fluorophores in a row is 4.3 nm, while the distance between each row is 6.8 nm (Figure 1b,c). The sensor modules, also called locks, keep the device in a closed state and the two arrays of FRET pairs in close proximity. Each of the four locks consists of two partly complementary DNA strands that form a 15 bp long duplex where one of the strands has a single-stranded toehold of 8 bases for binding of an oligonucleotide key of 23 bases. The key oligo first binds to the toehold and then displaces the shorter lock strand from the lock duplex *via* branch migration.[40,41] Upon addition of keys, the locks open, and the two panels move apart due to electrostatic repulsion of the DNA panels and the entropy of the system. The transition from a closed state to an open state increases the distance between donor and acceptor arrays resulting in a different fluorescence profile. The rectangular panels are designed as single-layered sheets with helices running vertically with respect to the foot, which is a rigid double-layered part of the structure (Figure 1a–c). This structure had the best performance out of the three designs that were tested. Two other prototypes of a multifluorophore FRET beacon were designed and assessed in order to test the stiffness of the panels, which could affect the position of the fluorophore arrays in relation to each other. A comparison of the three prototypes (Figure S1), blueprints (Figures S2–S4), structural characterization (Figures S5–S8), and sequences (Table S1–S3) are provided in the Supporting Information.

The DNA Origami Beacon Can Be Self-Assembled in Open and Closed States. The DNA origami beacon is a dynamic structure that can be assembled in either an open or closed state by excluding or including the lock staples in the self-assembly reaction, respectively. Electrophoretic gel analysis of structures assembled at 12 and 24 mM Mg^{2+} showed a significant electrophoretic shift between the structures assembled in open and closed states (Figure S5c). Furthermore, the structure assembled in the closed state at 24 mM Mg^{2+} has a slightly higher electrophoretic mobility compared to the same structure assembled at 12 mM Mg^{2+}, suggesting that structures are more compact. An AFM micrograph of the structure assembled in the open state at 12 mM Mg^{2+} shows two types of structures: a 6 nm tall square structure and a 2 nm tall rectangular structure with a 4 nm taller feature in the middle (Figure 1d). The square structure corresponds to a device in a closed state (Figure 1e, closed), while the rectangular structure corresponds to a device in open state with the protruding foot in the middle (Figure 1e, open). The dimensions of the DNA origami beacon correspond to theoretical values from the 3D model made in caDNAno.[39] The device measured 51.6 ± 3.3 nm × 44.4 ± 2.7 nm in the closed state and 54.6 ± 1.5 nm × 93.8 ± 4.1 nm in the open state (n = 20) compared with the theoretical values of 52 × 46 nm and 52 × 90 nm for the closed and open states, respectively. AFM imaging of devices assembled at 12 mM Mg^{2+} in the closed state showed that devices adsorb to the surface preferably in an open state and only few structures are observed in a closed state (Figure S6a). This could be due to electrostatic repulsion between the sheets or opening upon deposition on the mica surface. Increase of Mg^{2+} concentration during self-assembly reaction results in a higher yield of closed structures as determined by AFM (Figure S6b). Open structures adsorb to the surface in an open state when assembled at low Mg^{2+} concentration (Figure S6c); assembled at higher Mg^{2+} concentration, they are also observed in the closed conformation (Figure S6d). Both gel electrophoresis analysis and AFM analysis have shown that devices can be assembled in open and closed states and suggest that Mg^{2+} concentration plays an important role during the self-assembly of the structure in a closed state.

Determining the Optimal Mg^{2+} Concentration during Self-Assembly and Purification Steps. Mg^{2+} plays an important role during self-assembly of DNA nanostructures shielding the negative charge of phosphates, allowing duplex formation and tight packaging of the helices. We used FRET to assess the device in closed and open states to find the optimal Mg^{2+} concentration during the self-assembly and purification steps to achieve maximum signal difference between open and closed states (Figure S9). Oligos on corresponding rows of each panel were labeled in a one-pot reaction with either Cy3 or Cy5 conjugated ddUTP (Figure S10).[42] First, we assembled structures with one fluorophore row closest to the sensor modules in closed and open states at different Mg^{2+} concentrations in the range of 10–40 mM and found an optimal signal at 20 mM. Next, using 20 mM for self-assembly, we purified structures at different Mg^{2+} concentration in the range of 10–20 mM and found the optimal concentration for purification of the structures to be approximately 12 mM. The higher Mg^{2+} concentration during self-assembly serves to decrease the repulsion of the two panels and thus promotes self-assembly of the device in a closed state. However, higher concentration is not needed to keep the device closed after self-assembly. Reducing Mg^{2+} concentration during purification increases the repulsion between the panels, which is one of the driving forces in the opening mechanism resulting in a form of spring loading of the system. Interestingly, addition of more rows of fluorophores required higher Mg^{2+} concentrations, for example, optimal Mg^{2+} concentration for a device with four rows of FRET pairs was 30 mM (Figure S11) compared with 20 mM for a device with only one fluorophore row (Figure S9), while the optimal Mg^{2+} concentration during purification was approximately 12 mM (Figure S9). In conclusion, we identified the Mg^{2+} concentration requirements during self-assembly and purification steps in order to obtain optimal signal output from our sensor devices.

Optimization of DNA Origami Beacon Output Signal. The output signal of the device is a FRET difference between the closed and open states. The difference is generated during the opening of the device by increasing the distance between donor and acceptor fluorophore arrays. The foot of the device is a pivot point for the panels that are decorated with fluorophore arrays, and during the opening of the structure the two panels will pivot in opposite directions. The increased distance between the panels will be larger closer to the locks compared to the distance next to the foot and result in different FRET output for each rows of the device. The devices were assembled with one row of fluorophores per device to investigate how the fluorophore position on the structure affects signal output. The output signal of each row of fluorophores in the DNA origami beacon was examined by comparing the energy transfer difference between closed and open states of the device (Figure 2a). The three top rows have

DOI: 10.1021/acsnano.8b01510
ACS Nano 2018, 12, 5699–5708

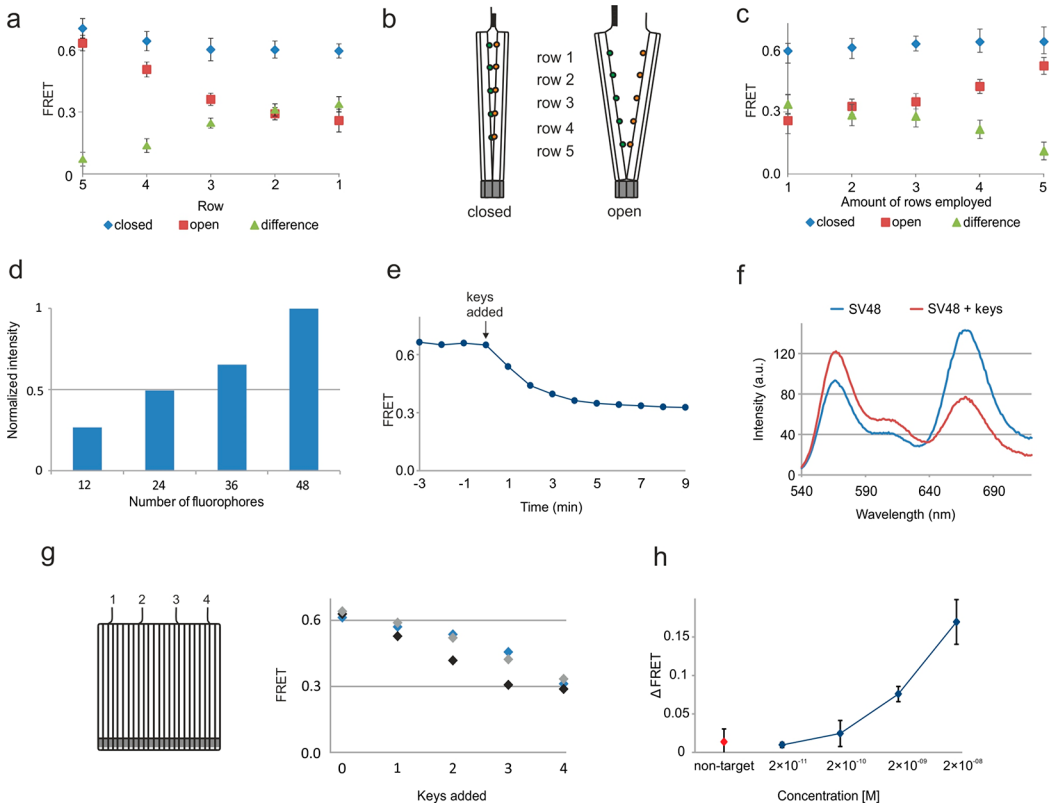

Figure 2. Ensemble fluorescence analysis of the DNA origami multifluorophore beacon. (a) Ensemble FRET characterization of performance of the individual fluorophore rows (n = 3). (b) Model of the closed and opened states based on the results in (a). (c) Ensemble FRET of beacons assembled with 1, 2, 3, 4, or 5 fluorophore rows (n = 3). (d) Normalized total fluorescence output signal intensity of 12, 24, 36, or 48 FRET pairs. All the beacons were assembled with 48 acceptors and either 12, 24, 36, or 48 donors. Fluorescence intensity at donor excitation was normalized to a directly excited acceptor intensity signal at 670 nm. (e) Time-resolved opening of the beacon with 48 FRET pairs. (f) Donor excited fluorescence spectra of a closed and open beacon with 48 FRET pairs. (g) Schematic representation of the locks position and opening of the beacon with 24 FRET pairs by sequential addition of the keys in different order: blue, 1, 2, 3, 4; gray, 1, 4, 2, 3; black, 2, 3, 4, 1. (h) Detection limit of the beacon with 48 FRET pairs in an ensemble fluorescence setup. FRET difference measured before and 6 min after addition of target DNA (n = 3).

similar energy transfer of around 0.6 in the closed state, the fourth row 0.65, while the bottom row closest to the foot has an energy-transfer output of 0.7. The open state energy transfer has a gradual increase from the row closest to the locks to the row next to the foot: from 0.3 to 0.6, respectively. This gives rise to varying FRET differences between closed and open state for different rows with a largest difference for the row closest to the locks of 0.3 to <0.1 for the row next to the pivot point. The smaller change in FRET difference at the bottom rows is a result of a smaller change in distance between the two panels closer to the foot (Figure 2b). The base stacking between the foot and panels probably prevents further opening of the device. Breaking up the base stacking by introducing a 7 bases single-stranded hinge resulted in a better opening of the structure, but at the expense of decreased FRET efficiency in the closed state as well as decreased FRET difference between the closed and open states (Figure S12). Although, the base stacking between the foot and the panels prevents complete opening of the device, it does play an important role in assembling the beacon in the closed state. The device without the single-stranded hinge provides a larger change in output signal and was used for the remaining experiments.

Larger Fluorophore Arrays Result in Increased Intensity Output Signal. We analyzed the DNA origami beacon with an increasing number of fluorophores to determine a maximum number of fluorophores while also achieving a maximum FRET difference (Figure 2c). The device was assembled with 1, 2, 3, 4, and 5 rows. The FRET difference for the beacons with 1, 2, and 3 rows was found to be about 0.3. Addition of the fourth and fifth rows decreased ΔFRET to around 0.23 and 0.12, respectively. Addition of the fifth row results in larger decrease of ΔFRET. A device with 4 rows decorated with a total of 48 FRET pairs has an optimal combination of the number of fluorophores while retaining a significant ΔFRET between the closed and open states. To determine the relationship between number of fluorophores and signal intensity, we assembled the DNA origami beacon with 48 acceptor fluorophores and various amount of donor fluorophores: 12, 24, 36, or 48 (Figure 2d). Increasing the amount of fluorophores resulted in a nearly linear increase in energy transfer output intensity with no self-quenching observed. This correlates with an earlier study where it was shown that the fluorescence intensity increases in a linear fashion with increasing number of fluorophores.[43] Combined these results demonstrate that signal change depends on which rows are decorated with FRET pairs and the signal intensity depends on how many fluorophores are employed. These data allowed us to choose optimal position and number of fluorophores to maximize the output: 4 rows with a total of 48 FRET pairs positioned closest to the sensor modules.

Effect of Sequential Opening and Determination of Detection Limit. The approach of using the DNA origami

DOI: 10.1021/acsnano.8b01510
ACS Nano 2018, 12, 5699−5708

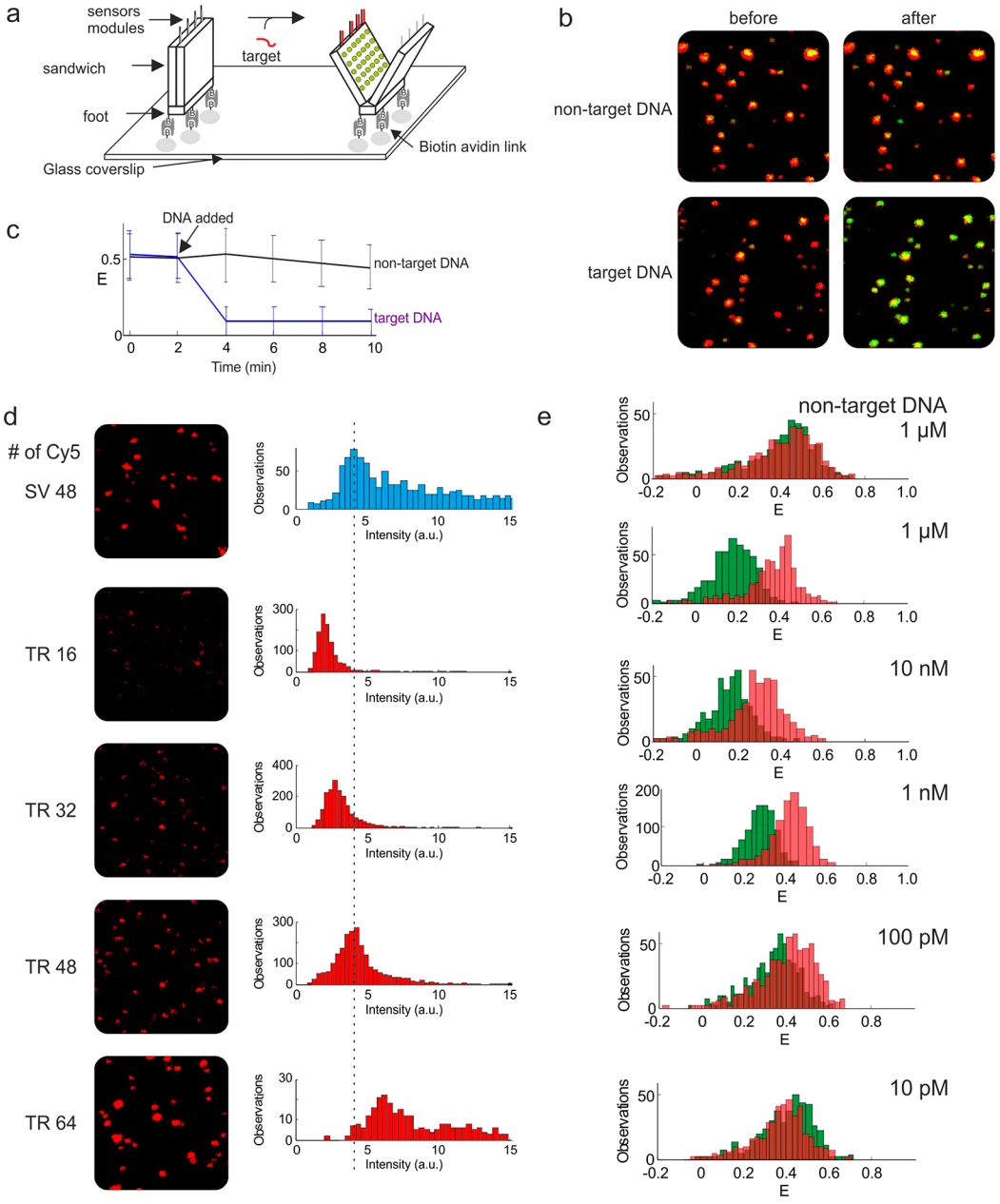

Figure 3. Single-device analysis of the DNA origami multifluorophore beacon. (a) Schematics of the attachment of the DNA origami beacon to a glass coverslip for single-device analysis showing the biotin–avidin linker. (b) Fluorescence images recorded before and 2 min after addition of nontarget or target DNA. Images show emission after donor excitation at 555 nm; green and red represent Cy3 and Cy5, respectively. Overlay of red and green is seen as yellow. Each image is 10.6 × 10.6 μm. (c) Time-resolved single-device analysis showing the average energy-transfer efficiency (E) of 1260 and 1254 particles in the scrambled and target DNA series, respectively. Error bars show SD. Raw images can be seen in Figure S14. (d) Rectangle origami labeled with 16, 32, 48, and 64 Cy5 fluorophores was used as a control for particle emission profiles. The beacon's Cy5 emission profile with 48 FRET pairs is shown in blue. Each image is 10.6 × 10.6 μm. (e) Detection limit of the beacon with 48 FRET pairs at a single-device level. The red and green histograms represent FRET efficiency distribution before and after addition of scrambled DNA (top) or target DNA at different concentrations. P-value for nontarget DNA and 10 pM > 0.5; p-values for the rest are <0.001.

beacon as a biosensor requires an opening of the device as a response to the input stimuli in a relatively short period of time. To determine the reaction time of the device with 48 FRET pairs, we performed an ensemble FRET time-resolved measurement of the DNA origami beacon in response to 100 pmol of DNA keys (Figure 2e). The time-resolved measurement shows an abrupt decrease in FRET efficiency with $T_{1/2}$ = 100s, where $T_{1/2}$ is time that takes to reach 50% of maximum FRET difference. Fluorescent profiles of the donor-excited emission of the beacon before and after addition of keys are shown in Figure 2f. We also analyzed the response of the device to each of the four keys by a sequential opening of the DNA origami beacon, where the keys were added one at a time in different sequential order (Figure 2g). The sequential opening revealed close to linear decrease in FRET during the opening of the structure by sequential addition of the keys. One of our other prototypes based on a more rigid 3D design showed more cooperativity between sensor modules and required

DOI: 10.1021/acsnano.8b01510
ACS Nano 2018, 12, 5699–5708

addition of two keys for some of the combinations to achieve significant FRET change (Figure S13). These results demonstrate that addition of one of the keys to the structure leads to its partial opening, enabling the device to detect four different targets simultaneously. The DNA origami beacon with 4 rows and a total of 48 FRET pairs was used to test the detection limit of the device using an ensemble fluorescence setup. The lowest significant FRET change compared with a nontarget DNA control was achieved at a target concentration of 2 nM after only 6 min (Figure 2h). Longer analysis time had no effect on the detection limit (Figure S14).

Single Beacon Analysis by Laser Scanning Microscope. The main idea of making a device where 48 FRET pairs work in concert was to make a biosensor platform that would allow detection of singular devices using a mainstream fluorescence microscope. The foot of the DNA origami beacon was functionalized with biotin molecules that allowed immobilization of the device on a coverslip covered by biotinylated bovine serum albumin (BSA) through an avidin molecule (Figure 3a). Immobilized devices were imaged every 2 min for a total of 10 min, and mismatch or target DNA was added after 2 min (Figure 3b). Data analysis shows the average FRET efficiency of 1260 and 1254 particles for mismatch and target DNA, respectively (Figure 3c). There is no change in the average FRET when adding nontarget DNA. Addition of the target DNA results in a significant change of the average FRET efficiency, which is also observable in the recorded images (Figure S15). The intensities of the fluorescence spots in the sample are not uniform, and the question is whether single devices or only aggregates of multiple devices are observed. A control experiment was conducted to address this question where Rothemund's original tall rectangle[18] was used as a control structure. Rothemund showed that omitting the staples on both long edges of the rectangle (Figure S16) abolishes the aggregation and singular structures can be observed.[18] Four tall rectangle structures were assembled with 16, 32, 48, and 64 Cy5 fluorophores, respectively. All structures were biotinylated to enable positioning onto the surface in the same manner as the DNA beacon. Structures were visualized and analyzed in the same way as the multi-FRET DNA beacon structures. Analysis of the structures containing 16, 32, and 48 fluorophores revealed only one intensity peak as a result of dispersion of singular rectangles on the surface (Figure 3d). The width of distribution of the peaks is a result of incomplete TdT enzyme labeling of the oligos (Figure S10). The sample with 64 Cy5 resulted in one main peak; though, some degree of oligomerization was observed probably due to hydrophobic contact between Cy5 molecules.[44] Increasing fluorescence intensity with increasing number of fluorophores recorded by fluorescence microscopy correlates with a previous study.[43] Importantly, the peak position of the tall rectangle sample labeled with 48 fluorophores coincides with the main peak of the DNA beacon labeled with 48 FRET pairs, proving that singular devices are observed. Based on the identification of singular devices the signals were sorted into signals coming from single, double, and multiple devices (Figure S17). The most intense signals showed very small changes between closed and open conformations. These spots probably present large aggregates of poorly assembled structures, as their initial FRET value is much lower compared to other groups. The self-assembly yield is very high, resulting in more than 93% of functional structures (see Figure S17). The results demonstrate that the DNA beacon can be used as a biosensor platform in a conventional fluorescence microscope setup allowing analysis of hundreds of devices simultaneously on a single-device level.

Lower Limit of Detection from Singular DNA Beacon Analysis. Adsorption of the devices to the surface in a single-beacon experiment results in much lower device concentration as non-adsorbed structures are washed away. This leads to a higher effective concentration of the keys per device compared to the ensemble FRET experiments. Furthermore, the ability to detect an analyte on single device level results in a high statistical significance, as each device can now be considered an independent experiment. To test this, we assessed the detection limit of the DNA beacon in a single device setup. Addition of target DNA in concentrations down to 100 pM resulted in a significant FRET change with p-value <0.001 (Figure 3e). This is compared with the ensemble FRET measurements where we could detect down to 2 nM concentration of the keys (Figure S18). The combined analysis of the sample takes 40−60 min, including microscopy and statistical analysis of the data, which is comparable to current state-of-the-art mechanical biosensors.[45] These results demonstrate the power of single device analysis using a conventional fluorescence microscope setup detecting concentration of nucleic acids down to 100 pM.

CONCLUSION

Here, we have presented the design and construction of a DNA origami nanostructure functioning as a multiple FRET pair beacon with a strong fluorescence output that can be used to analyze singular devices using a mainstream fluorescence microscope setup without the need for a specialized single-molecule setup. Our idea exploits ordered organic fluorophore arrays, where two of these arrays, one with donor fluorophores and one with acceptor fluorophores, create a multi-FRET pair. The multi-FRET pair is used in the device to detect molecular events without the need for external labeling procedures. Furthermore, the acceptor array could be exchanged for a quencher array allowing the "off−on" detection of the signal.

Self-assembly of the device was optimized using FRET as output signal. Device conformation *in situ* and optimal number of fluorophores in the arrays were determined by ensemble FRET. We have shown the power of single-molecule analysis by analyzing thousands of particles simultaneously that provides large data sets making the statistical comparison of the two states of the device more accurate, which resulted in a detection of target nucleic acid sequences in concentrations down to 100 pM. Rothemund's tall rectangle with various amounts of fluorophores was used as a fluorescence microscopy calibration control to determine that singular devices were detected on the surface.

In conclusion, we have demonstrated a general-purpose sensor platform for linear label-free signal amplification that delivers an output signal detectable with a mainstream fluorescence confocal microscope setup. In the future, the sensor platform may be further developed to improve sensitivity, acquisition time, and range of targets detected. Recently, it has been reported that localized cascade DNA hybridization chain reactions[46] on DNA origami platforms improves biosensing properties and such cascades could be easily integrated into the sensor modules of the DNA origami beacon. Another way to improve sensitivity and response time is to automate the data acquisition and analysis to remove nonfunctional sensor signals and analyze large amounts of sensor devices. To expand the range of targets for detection, DNA locks could be exchanged for aptamer locks and

DOI: 10.1021/acsnano.8b01510
ACS Nano 2018, 12, 5699−5708

programmed to recognize different targets such as proteins and small molecules.[24,47] The biosensor platform could be developed for multiplex analysis by constructing barcodes of unique donor−acceptor dye combinations to obtain specifically tuned emission profiles, which would allow the detection of hundreds of different targets in the same sample.

METHODS

Design Tools. CadNano software (http://cadnano.org/) was a primary design tool used for generation of staple strand sequences. CadNano plugin in AutoCAD Maya (http://www.autodesk.com/) was used for evaluation of the 3D shape and dynamics. Designed structures were evaluated for local flexibility and strain using online based software tool CanDo (http://cando-dna-origami.org/).

Self-Assembly of DNA Structures. The self-assembly of DNA origami structures was performed by mixing M13 ssDNA (M13mp18, Bayou Biolabs) with 5× excess of staple strands in 100 μL TAE/Mg^{2+} buffer (40 mM Trisacetate, 1 mM EDTA, pH = 8.3, 8−50 mM Mg^{2+}). Annealing of staple strands was done using a temperature ramp: 65 °C for 20 min, followed by a temperature decrease of 0.1 °C/6 min until 40 °C.

Nucleotide Conjugation to Cy3 and Cy5 Fluorophores. Phosphate-buffered saline (135 mM NaCl, 2.7 mM KCl, 8 mM $Na_2HPO_4{\cdot}2\ H_2O$, and 2 mM KH_2PO_4, pH 7.4) was mixed with 0.2 M sodium bicarbonate solution (pH 9.0) in a 20:1 ratio with a final pH of 8.3. 5-Propargylamino-ddUTP (Jena Bioscience, Germany) was added to the mix to final concentration of 0.5 mM. Cy3-NHS or Cy5-NHS (Lumiprobe, Germany) was added in 10× excess to nucleotide. Reaction was incubated for 1 h at room temperature, protected from light by tinfoil. The conjugate was purified by HPLC (Agilent technologies, USA) using XB-C18 reverse phase column (Phenomenex), lyophilized, and dissolved in water. The integrity of the conjugate was confirmed by terminal transferase assay.

HPLC Purification. Labeled oligonucleotides and nucleotides were HPLC purified using Agilent 1200 HPLC system (Agilent technologies, USA) and Kinetex 2.6 μm XB C18 150 × 4.6 mm reverse phase column (Phenomenex). Collected peaks were freeze-dried to concentrate the sample. Lastly, the oligo was dissolved in water, and sample concentration was measured.

Terminal Transferase (TdT) Labeling of Oligonucleotides. Unmodified staple strands were purchased from DNA Technology A/S (Risskov, Denmark) at a concentration 100 μM. The selected oligonucleotides at donor and acceptor FRET pair positions were labeled either with ddUTP-Cy3 or ddUTP-Cy5 conjugates. Standard TdT reaction includes 100 pmol oligonucleotide in total and 500 pmol of modified ddUTP mixed in 20 μL with reaction buffer (1×) and $CoCl_2$ (5 mM) and incubated with terminal transferase (20 U/μL) for half of 45 min at 37 °C. The reaction was stopped by incubating the sample mix at 70 °C for 10 min. Strands were either used directly for origami structure self-assembly or added EDTA (20 mM final concentration) and precipitated with NaOAc (0.3 M, pH = 5.2) and 2.5 volumes of 96% EtOH for 30 min on dry ice, followed by centrifugation for 30 min at 15,000 *g*. The pellet was washed twice with 70% EtOH dried and dissolved in water. These were then used for self-assembly or HPLC purified using XB-C18 reverse phase column.

Biotinylated oligonucleotides for the foot of the beacons were prepared the same way using biotin-16- dUTP (Jena Bioscience, Germany).

Polyacrylamide Gel Mobility Shift Assays. Labeled oligonucleotides were analyzed using polyacrylamide gel by comparing gel shift to unlabeled product. Standard 14% polyacrylamide gels were prepared using SequaGel system (National Diagnostics, USA). Gels were prerun for 20 min prior to loading the samples containing 10% formamide. Samples were run for 1 h at 25 W at room temperature. Gels were visualized directly with Typhoon Trio+ scanner (GE Healthcare Life Sciences) or stained with 1× SYBR Gold prior visualization.

Agarose Gel Mobility Shift Assays. Self-assembled DNA structures were used directly or purified prior to loading onto the gel. The DNA structure samples were loaded onto the 1% agarose gel containing 5 mM Mg^{2+} and allowed to migrate for 4 h in a cold room at 70 V. The gel was stained with 1× SYBR Safe for 30 min, and migrated bands were visualized with BioRad Gel Doc EZ scanner.

Structure Purification. DNA structures were assembled with 5× excess of staple strands. Unincorporated staple strands were removed prior to further analysis and experiments. Two purification methods were employed either with MicroSpin S-400 HR (GE Healthcare Life Sciences, USA) or with 100k Amicon Ultra-0.5 mL centrifugal filters (Millipore, Germany).

MicroSpin protocol was followed using annealing buffer (TAE/Mg^{2+} buffer) for column wash. At least two rounds of purifications were needed to remove excess of staple strands.

Amicon filters were prewet with annealing buffer by loading 500 μL of buffer onto the filter and centrifuging at 1800 RCF for 9 min. Sample was loaded on the filter and filled with the annealing buffer up to total volume of 500 μL and spun at the 1800 RCF for 9 min, washed twice with 500 μL of annealing buffer 9 min each time, and eluted during 2 min.

AFM Imaging. Freshly cleaved mica was incubated with annealing buffer TAE/12 mM Mg^{2+} for a few minutes prior to deposition of the purified sample (3−8 μL of 2−10 nM). Two AFMs were used for imaging: an Agilent AFM series 5500 (Agilent Technologies, USA) and Multimode VIII AFM (Veeco Instruments, Santa Barbara, USA) with 0.08 N/m force constant silicon nitride cantilevers with sharpened pyramidal tip (Veeco Probes, Camarillo, USA). All images were analyzed using NanoScope analysis software.

TEM Imaging. Carbon grids (Formvar/Carbon coated grids (SPI # 3440C)) were glow discharged at 25 mA for 30 s, 0.25 mbar. A sample (5 μL, 10 nM) was incubated on the grid for 1 min and excess of sample mix removed. The grid was incubated with a 2% aqueous uranyl formate with 25 mM NaOH stain solution for 1 min, and excess of stain solution was removed. Imaging was done on TEM CM120 (Philips) machines.

Ensemble Fluorescence Measurement. Self-assembled, purified structures (50 μL, 0.1 nM) were loaded in a quartz cuvette with a volume of 60 μL (Hellma). Fluorescence spectra of the different beacons were recorded with a spectrofluorometer (FluoroMax-3 from HORIBA Jobin Yvon) after excitation of donor fluorophores at 530 nm and of acceptor fluorophores at 630 nm.

Zeiss Laser Scanning Microscope 700 Imaging. A flow cell was made consisting of a glass slide, coverslip, and parafilm. The glass slide was covered with parafilm where a 20 mm-wide channel was cut with a razor. The glass coverslip was placed onto the parafilm, and the whole flow cell was heated on a heat block until the parafilm became soft and the coverslip stuck to it. Below is a schematic representation of the homemade flow cell:

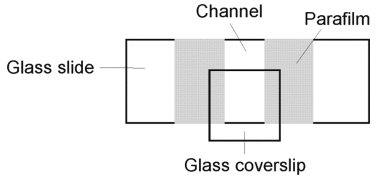

The flow cell channel was incubated with 40 μL of 75 μM biotinylated bovine serum albumin (Sigma-Aldrich, USA) solution in water for 5 min at room temperature, washed with TAE/11 mM Mg^{2+} buffer, incubated with 40 μL of 1.5 μM avidin (Sigma-Aldrich, USA) solution in water for 5 min at room temperature, and washed with TAE/11 mM Mg^{2+} buffer. Biotinylated DNA origami samples 20 μL of 0.5−1 nM in TAE/11 mM Mg^{2+} were then added to the flow cell for 5 min at room temperature, washed with TAE/30 mM Mg^{2+} buffer, washed again with antibleaching buffer (1 × TAE, 30 mM Mg^{2+}, 150 mM Na^+, 2 mM 6-hydroxy-2,5,7,8-tetramethylchroman-2-carboxylic acid (Trolox), 2600 units/mL of catalase, and 166 units/ml of glucose oxidase and 25 mM glucose).

DOI: 10.1021/acsnano.8b01510
ACS Nano 2018, 12, 5699−5708

Samples were imaged using 555 and 639 nm lasers at 1 mW for Cy3 and Cy5 direct excitations, respectively. Images were taken in sequence of 6 images recorded every 1−2 min. After direct excitation of Cy3, two data sets were collected using two channels: one for Cy3 emission and one for Cy5 emission. Direct excitation of Cy5 resulted in one data set of Cy5 emission.

Data Analysis for Microscopy Experiments. Data analysis was performed using custom built software ImageA in MatLab (MathWorks). The software allowed finding fluorescence particles peaks in the microscope image and extracting their intensity in each image of the sequence. Furtheremore, position drifts as a function of time were corrected. It is possible to divide particles in different groups depending on their intensity and particle size and set limits of the size of the particle and threshold intensity of the pixel to differ the background from the signal. Many of these features are also implemented in the single molecule FRET iSMS software.[48]

Correction Factors for FRET Calculations. Structures labeled with either 48 Cy5 molecules or with 48 Cy3 molecules were assembled and purified. Emission spectra recorded as described in "Zeiss Laser Scanning Microscope 700 imaging". Data are shown in Table S4. Donor bleedthrough is calculated using data recorded for structures labeled only with Cy3 molecules:

$$D_{bt} = \frac{F_D(\lambda_A^{Em})}{F_D(\lambda_D^{Em})}$$

where $F_D(\lambda_A^{Em})$ is the intensity at acceptor wavelength when excited at donor wavelength and $F_D(\lambda_D^{Em})$ is the intensity at donor wavelength when excited at donor wavelength.

Donor fluorescence at acceptor wavelength when excited at acceptor wavelength was not significant (<1%).

Direct acceptor excitation by donor wavelength was calculated using data recorded for structure labeled only with Cy5 molecules:

$$A_{de} = \frac{F_D(\lambda_A^{Em})}{F_A(\lambda_A^{Em})}$$

where $F_D(\lambda_A^{Em})$ is the intensity at acceptor wavelength when excited at donor wavelength and $F_A(\lambda_A^{Em})$ is the intensity at donor wavelength when excited at donor wavelength.

Energy-Transfer Calculations. Energy-transfer efficiency calculations for ensemble fluorescence measurements where the donor is excited and both the donor and acceptor intensities are measured:

$$E = \frac{I_A}{I_A + I_D}$$

where E is energy-transfer efficiency, I_A is acceptor intensity, and I_D is donor intensity.

Energy-transfer efficiency for single-molecule analysis was calculated by

$$E = \frac{F_D(\lambda_A^{Em}) - F_A(\lambda_A^{Em}) \times A_{de} - F_D(\lambda_D^{Em}) \times D_{bt}}{F_D(\lambda_D^{Em}) + (F_D(\lambda_A^{Em}) - F_A(\lambda_A^{Em}) \times A_{de} - F_D(\lambda_D^{Em}) \times D_{bt})}$$

where $F_D(\lambda_A^{Em})$ is the intensity at acceptor wavelength when excited at donor wavelength, $F_D(\lambda_D^{Em})$ is the intensity at donor wavelength when excited at donor wavelength, $F_A(\lambda_A^{Em})$ is the intensity at donor wavelength when excited at donor wavelength, and A_{de} and D_{bt} are measured correction factors as given in Table S1.

ASSOCIATED CONTENT

Supporting Information

The Supporting Information is available free of charge on the ACS Publications website at DOI: 10.1021/acsnano.8b01510.

Comparison of design of three prototypes and caDNAno blueprints (Figures S1−S4), respectively. Gel electrophoresis analysis (Figure S5). AFM (Figures S6 and S8) and TEM (Figure S7) characterization of the three prototype structures. Figure S9 represents ensemble FRET characterization of assembly and mechanical opening of the three prototypes. One-pot labeling efficiency with TdT enzyme is demonstrated in Figure S10. Mg^{2+} optimization for biosensor with 48 FRET pairs with and without hinge is shown in Figures S11 and S12, respectively. Data for sequential opening of three prototypes are shown in Figure S13. Limit of detection of ensemble experiment after different time points plotted on one graph is depicted in Figure S14. Microscopy data of opening of biosensor with 48 FRET pairs as a response to different input oligos is found as Figure S15. Design blueprint of tall rectangle structure that was used as a control for microscopy experiments is shown in Figure S16. Figure S17 shows single-particle analysis of the sample where data of all particles are divided into several groups: singular devices, doublets, small, medium, and large oligomers. Comparison of limit of detection of ensemble and single device data is included in Figure S18. Oligo sequences used for assembly of three prototypes are listed in Tables S1−S3, respectively. Table S4 shows correction factors used for calculations of FRET values in single molecule experiments (PDF)

AUTHOR INFORMATION

Corresponding Author

*E-mail: esa@inano.au.dk.

ORCID

Victoria Birkedal: 0000-0002-1360-8870

Ebbe Sloth Andersen: 0000-0002-6236-8164

Notes

The authors declare no competing financial interest.

ACKNOWLEDGMENTS

The authors acknowledge support from the Danish Council for Independent Research (grant number 0602-01772B to E.S.A.) and (grant number 0602-01670B to V.B.).

REFERENCES

(1) Sheng, Q.; Liu, R.; Zhang, S.; Zheng, J. Ultrasensitive Electrochemical Cocaine Biosensor Based on Reversible DNA Nanostructure. *Biosens. Bioelectron.* **2014**, *51*, 191−194.

(2) Farjami, E.; Campos, R.; Nielsen, J. S.; Gothelf, K. V.; Kjems, J.; Ferapontova, E. E. RNA Aptamer-Based Electrochemical Biosensor for Selective and Label-Free Analysis of Dopamine. *Anal. Chem.* **2013**, *85*, 121−128.

(3) Jepsen, M. D. E.; Sparvath, S. M.; Nielsen, T. B.; Langvad, A. H.; Grossi, G.; Gothelf, K. V.; Andersen, E. S. Development of a Genetically Encodable FRET System Using Fluorescent RNA Aptamers. *Nat. Commun.* **2018**, *9*, 18.

(4) Wang, J.; Liu, J.; Thomsen, J.; Selnihhin, D.; Hede, M. S.; Kirsebom, F. C.; Franch, O.; Fjelstrup, S.; Stougaard, M.; Ho, Y. P.; Pedersen, F. S.; Knudsen, B. R. Novel DNA Sensor System for Highly Sensitive and Quantitative Retrovirus Detection Using Virus Encoded Integrase as a Biomarker. *Nanoscale* **2017**, *9*, 440−448.

(5) Bertolin, G.; Sizaire, F.; Herbomel, G.; Reboutier, D.; Prigent, C.; Tramier, M. A Fret Biosensor Reveals Spatiotemporal Activation and Functions of Aurora Kinase a in Living Cells. *Nat. Commun.* **2016**, *7*, 12674.

(6) Rodriguez-Lorenzo, L.; de la Rica, R.; Alvarez-Puebla, R. A.; Liz-Marzan, L. M.; Stevens, M. M. Plasmonic Nanosensors with Inverse Sensitivity by Means of Enzyme-Guided Crystal Growth. *Nat. Mater.* **2012**, *11*, 604−607.

DOI: 10.1021/acsnano.8b01510
ACS Nano 2018, 12, 5699−5708

(7) Backmann, N.; Zahnd, C.; Huber, F.; Bietsch, A.; Pluckthun, A.; Lang, H. P.; Guntherodt, H. J.; Hegner, M.; Gerber, C. A Label-Free Immunosensor Array Using Single-Chain Antibody Fragments. *Proc. Natl. Acad. Sci. U. S. A.* **2005**, *102*, 14587−14592.
(8) Miyawaki, A.; Llopis, J.; Heim, R.; McCaffery, J. M.; Adams, J. A.; Ikura, M.; Tsien, R. Y. Fluorescent Indicators for Ca2+ Based on Green Fluorescent Proteins and Calmodulin. *Nature* **1997**, *388*, 882−887.
(9) Cybulski, J. S.; Clements, J.; Prakash, M. Foldscope: Origami-Based Paper Microscope. *PLoS One* **2014**, *9*, e98781.
(10) Miller, A. R.; Davis, G. L.; Oden, Z. M.; Razavi, M. R.; Fateh, A.; Ghazanfari, M.; Abdolrahimi, F.; Poorazar, S.; Sakhaie, F.; Olsen, R. J.; Bahrmand, A. R.; Pierce, M. C.; Graviss, E. A.; Richards-Kortum, R. Portable, Battery-Operated, Low-Cost, Bright Field and Fluorescence Microscope. *PLoS One* **2010**, *5*, e11890.
(11) Ming, K.; Kim, J.; Biondi, M. J.; Syed, A.; Chen, K.; Lam, A.; Ostrowski, M.; Rebbapragada, A.; Feld, J. J.; Chan, W. C. W. Integrated Quantum Dot Barcode Smartphone Optical Device for Wireless Multiplexed Diagnosis of Infected Patients. *ACS Nano* **2015**, *9*, 3060−3074.
(12) Kuhnemund, M.; Wei, Q.; Darai, E.; Wang, Y.; Hernandez-Neuta, I.; Yang, Z.; Tseng, D.; Ahlford, A.; Mathot, L.; Sjoblom, T.; Ozcan, A.; Nilsson, M. Targeted DNA Sequencing and *in situ* Mutation Analysis Using Mobile Phone Microscopy. *Nat. Commun.* **2017**, *8*, 13913.
(13) Wei, Q.; Luo, W.; Chiang, S.; Kappel, T.; Mejia, C.; Tseng, D.; Chan, R. Y.; Yan, E.; Qi, H.; Shabbir, F.; Ozkan, H.; Feng, S.; Ozcan, A. Imaging and Sizing of Single DNA Molecules on a Mobile Phone. *ACS Nano* **2014**, *8*, 12725−12733.
(14) Liu, J.; Yang, X.; Wang, K.; Wang, Q.; Liu, W.; Wang, D. Solid-Phase Single Molecule Biosensing Using Dual-Color Colocalization of Fluorescent Quantum Dot Nanoprobes. *Nanoscale* **2013**, *5*, 11257−11264.
(15) Zhang, C. Y.; Hu, J. Single Quantum Dot-Based Nanosensor for Multiple DNA Detection. *Anal. Chem.* **2010**, *82*, 1921−1927.
(16) Vietz, C.; Kaminska, I.; Sanz Paz, M.; Tinnefeld, P.; Acuna, G. P. Broadband Fluorescence Enhancement with Self-Assembled Silver Nanoparticle Optical Antennas. *ACS Nano* **2017**, *11*, 4969−4975.
(17) Ochmann, S. E.; Vietz, C.; Trofymchuk, K.; Acuna, G. P.; Lalkens, B.; Tinnefeld, P. Optical Nanoantenna for Single Molecule-Based Detection of Zika Virus Nucleic Acids without Molecular Multiplication. *Anal. Chem.* **2017**, *89*, 13000−13007.
(18) Rothemund, P. W. Folding DNA to Create Nanoscale Shapes and Patterns. *Nature* **2006**, *440*, 297−302.
(19) Andersen, E. S.; Dong, M.; Nielsen, M. M.; Jahn, K.; Lind-Thomsen, A.; Mamdouh, W.; Gothelf, K. V.; Besenbacher, F.; Kjems, J. DNA Origami Design of Dolphin-Shaped Structures with Flexible Tails. *ACS Nano* **2008**, *2*, 1213−1218.
(20) Douglas, S. M.; Dietz, H.; Liedl, T.; Hogberg, B.; Graf, F.; Shih, W. M. Self-Assembly of DNA into Nanoscale Three-Dimensional Shapes. *Nature* **2009**, *459*, 414−418.
(21) Zhang, F.; Jiang, S.; Wu, S.; Li, Y.; Mao, C.; Liu, Y.; Yan, H. Complex Wireframe DNA Origami Nanostructures with Multi-Arm Junction Vertices. *Nat. Nanotechnol.* **2015**, *10*, 779−784.
(22) Andersen, E. S.; Dong, M.; Nielsen, M. M.; Jahn, K.; Subramani, R.; Mamdouh, W.; Golas, M. M.; Sander, B.; Stark, H.; Oliveira, C. L.; Pedersen, J. S.; Birkedal, V.; Besenbacher, F.; Gothelf, K. V.; Kjems, J. Self-Assembly of a Nanoscale DNA Box with a Controllable Lid. *Nature* **2009**, *459*, 73−76.
(23) Zadegan, R. M.; Jepsen, M. D.; Thomsen, K. E.; Okholm, A. H.; Schaffert, D. H.; Andersen, E. S.; Birkedal, V.; Kjems, J. Construction of a 4 Zeptoliters Switchable 3d DNA Box Origami. *ACS Nano* **2012**, *6*, 10050−10053.
(24) Douglas, S. M.; Bachelet, I.; Church, G. M. A Logic-Gated Nanorobot for Targeted Transport of Molecular Payloads. *Science* **2012**, *335*, 831−834.
(25) Marras, A. E.; Zhou, L.; Su, H. J.; Castro, C. E. Programmable Motion of DNA Origami Mechanisms. *Proc. Natl. Acad. Sci. U. S. A.* **2015**, *112*, 713−718.
(26) Grossi, G.; Dalgaard Ebbesen Jepsen, M.; Kjems, J.; Andersen, E. S. Control of Enzyme Reactions by a Reconfigurable DNA Nanovault. *Nat. Commun.* **2017**, *8*, 992.
(27) Melinger, J. S.; Khachatrian, A.; Ancona, M. G.; Buckhout-White, S.; Goldman, E. R.; Spillmann, C. M.; Medintz, I. L.; Cunningham, P. D. Fret from Multiple Pathways in Fluorophore-Labeled DNA. *ACS Photonics* **2016**, *3*, 659−669.
(28) Hemmig, E. A.; Creatore, C.; Wunsch, B.; Hecker, L.; Mair, P.; Parker, M. A.; Emmott, S.; Tinnefeld, P.; Keyser, U. F.; Chin, A. W. Programming Light-Harvesting Efficiency Using DNA Origami. *Nano Lett.* **2016**, *16*, 2369−2374.
(29) Buckhout-White, S.; Spillmann, C. M.; Algar, W. R.; Khachatrian, A.; Melinger, J. S.; Goldman, E. R.; Ancona, M. G.; Medintz, I. L. Assembling Programmable Fret-Based Photonic Networks Using Designer DNA Scaffolds. *Nat. Commun.* **2014**, *5*, 5615.
(30) Diaz, S. A.; Buckhout-White, S.; Ancona, M. G.; Spillmann, C. M.; Goldman, E. R.; Melinger, J. S.; Medintz, I. L. Extending DNA-Based Molecular Photonic Wires with Homogeneous Forster Resonance Energy Transfer. *Adv. Opt. Mater.* **2016**, *4*, 399−412.
(31) Li, Y.; Du, H.; Wang, W.; Zhang, P.; Xu, L.; Wen, Y.; Zhang, X. A Versatile Multiple Target Detection System Based on DNA Nano-Assembled Linear Fret Arrays. *Sci. Rep.* **2016**, *6*, 26879.
(32) Tyagi, S.; Kramer, F. R. Molecular Beacons: Probes That Fluoresce Upon Hybridization. *Nat. Biotechnol.* **1996**, *14*, 303−308.
(33) Ke, Y.; Lindsay, S.; Chang, Y.; Liu, Y.; Yan, H. Self-Assembled Water-Soluble Nucleic Acid Probe Tiles for Label-Free RNA Hybridization Assays. *Science* **2008**, *319*, 180−183.
(34) Tintore, M.; Gallego, I.; Manning, B.; Eritja, R.; Fabrega, C. DNA Origami as a DNA Repair Nanosensor at the Single-Molecule Level. *Angew. Chem., Int. Ed.* **2013**, *52*, 7747−7750.
(35) Kuzuya, A.; Sakai, Y.; Yamazaki, T.; Xu, Y.; Komiyama, M. Nanomechanical DNA Origami 'Single-Molecule Beacons' Directly Imaged by Atomic Force Microscopy. *Nat. Commun.* **2011**, *2*, 449.
(36) Nickels, P. C.; Hoiberg, H. C.; Simmel, S. S.; Holzmeister, P.; Tinnefeld, P.; Liedl, T. DNA Origami Seesaws as Comparative Binding Assay. *ChemBioChem* **2016**, *17*, 1093−1096.
(37) Wang, D.; Vietz, C.; Schroder, T.; Acuna, G.; Lalkens, B.; Tinnefeld, P. A DNA Walker as a Fluorescence Signal Amplifier. *Nano Lett.* **2017**, *17*, 5368−5374.
(38) Nickels, P. C.; Wunsch, B.; Holzmeister, P.; Bae, W.; Kneer, L. M.; Grohmann, D.; Tinnefeld, P.; Liedl, T. Molecular Force Spectroscopy with a DNA Origami-Based Nanoscopic Force Clamp. *Science* **2016**, *354*, 305−307.
(39) Douglas, S. M.; Marblestone, A. H.; Teerapittayanon, S.; Vazquez, A.; Church, G. M.; Shih, W. M. Rapid Prototyping of 3d DNA-Origami Shapes with Cadnano. *Nucleic Acids Res.* **2009**, *37*, 5001−5006.
(40) Biswas, I.; Yamamoto, A.; Hsieh, P. Branch Migration through DNA Sequence Heterology. *J. Mol. Biol.* **1998**, *279*, 795−806.
(41) Zhang, D. Y.; Seelig, G. Dynamic DNA Nanotechnology Using Strand-Displacement Reactions. *Nat. Chem.* **2011**, *3*, 103−113.
(42) Sorensen, R. S.; Okholm, A. H.; Schaffert, D.; Kodal, A. L.; Gothelf, K. V.; Kjems, J. Enzymatic Ligation of Large Biomolecules to DNA. *ACS Nano* **2013**, *7*, 8098−8104.
(43) Schmied, J. J.; Raab, M.; Forthmann, C.; Pibiri, E.; Wunsch, B.; Dammeyer, T.; Tinnefeld, P. DNA Origami-Based Standards for Quantitative Fluorescence Microscopy. *Nat. Protoc.* **2014**, *9*, 1367−1391.
(44) Kang, J.; Kaczmarek, O.; Liebscher, J.; Dahne, L. Prevention of H-Aggregates Formation in Cy5 Labeled Macromolecules. *Int. J. Polym. Sci.* **2010**, *2010*, 264781.
(45) Arlett, J. L.; Myers, E. B.; Roukes, M. L. Comparative Advantages of Mechanical Biosensors. *Nat. Nanotechnol.* **2011**, *6*, 203−215.
(46) Bui, H.; Shah, S.; Mokhtar, R.; Song, T.; Garg, S.; Reif, J. Localized DNA Hybridization Chain Reactions on DNA Origami. *ACS Nano* **2018**, *12*, 1146−1155.

DOI: 10.1021/acsnano.8b01510
ACS Nano 2018, 12, 5699−5708

(47) Monserud, J. H.; Macri, K. M.; Schwartz, D. K. Toehold-Mediated Displacement of an Adenosine-Binding Aptamer from a DNA Duplex by Its Ligand. *Angew. Chem., Int. Ed.* **2016**, *55*, 13710−13713.
(48) Preus, S.; Noer, S. L.; Hildebrandt, L. L.; Gudnason, D.; Birkedal, V. iSMS: Single-Molecule FRET Microscopy Software. *Nat. Methods* **2015**, *12*, 593−594.

DOI: 10.1021/acsnano.8b01510
ACS Nano 2018, 12, 5699−5708